



ELSEVIER

Combustion and Flame 134 (355–368)

Combustion
and Flame

Effects of heat release in laminar diffusion flames lifted on round jets

Joan Boulanger^a, Luc Vervisch^{a,*}, Julien Reveillon^a, Sandip Ghosal^b

^aINSA and UMR 6614-CNRS-CORIA, Avenue de l'Université-BP8, 76801, Saint Etienne du Rouvray Cedex, France

^bNorthwestern University, Mechanical Engineering, Evanston, Illinois, USA

Received 15 March 2002; received in revised form 9 February 2003; accepted 5 May 2003

Abstract

Laminar diffusion flames lifted on round jets are simulated using high order accurate numerical schemes. The results are examined in the light of analytical approximations of lift-off heights. A large variety of flame base topologies are observed when the fuel jet velocity is varied. Edge-flames, or triple-flames, progressively evolve into weakly varying partially premixed fronts, before blow-out occurs. The flame base is located on the stoichiometric surface at the point where the flow velocity is of the order of the stoichiometric and planar premixed flame burning velocity. In the simulations, this stabilization point is positioned further upstream than predicted by a frozen flow mixing description of the jet, even when effects of heat release and strain rate are included in the approximation of the triple-flame speed that is used to predict the lift-off height. The numerical results therefore suggest that the well known flow deflection, induced by heat release, brings the flame much closer to the burner than expected. Heat release is found to have a much stronger effect in the round jet than in the previously studied planar mixing layer. In the axisymmetric problem, this is attributed to the intricate coupling between the flow deflection and the position of iso-mixture fraction surfaces relatively to iso-velocity surfaces. Heat release also makes the flame base more robust than predicted by cold flow theory and helps to sustain large velocities before reaching the blow-out condition. Results suggest that the prediction of lift-off height cannot be reached without carefully accounting for the effect of heat release on the flow upstream of the flame base. © 355–368 The Combustion Institute. All rights reserved.

Keywords: Lifted flame; Partially premixed combustion; Triple-flame; Edge-flame; Heat release

1. Introduction

Combustion in nonpremixed systems does not always start at the location where fuel and oxidizer first come into contact under stoichiometric conditions. In many practical devices, a large variety of conditions exist where the main burning zones are lifted away from the injection area of fuel and oxidizer. Frozen flow mixing occurs prior to ignition, and combustion is initiated in a partially premixed burning mode.

Sometimes, reactants are also mixed with recirculating hot products before burning. In this context, flames lifted in turbulent flows have been the subject of multiple studies to determine the exact control parameters of the turbulent flame base [1–4].

In laminar flows, triple-flames (also called edge-flames or tribrachial-flames) are observed when the flame is lifted in a two-dimensional planar mixing layer [5]. These planar triple-flames were studied in experiments [6–8], through theoretical analysis [9–15], as well as numerical simulations [16,17]. It was found that the speed of the triple-flame is controlled by two parameters: the curvature of the par-

* Corresponding author.

E-mail address: vervisch@coria.fr (L. Vervisch).

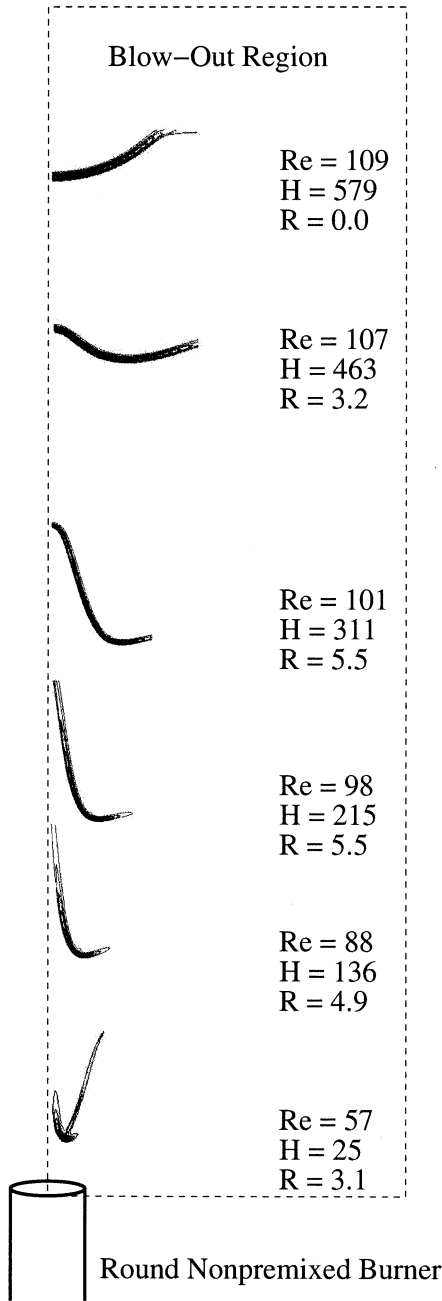


Fig. 1. Lift-off simulations for different jet Reynolds numbers. Flame bases are represented through their heat release rate. Re: Jet Reynolds number. H: Normalized lift-off height. R: Normalized radial position. The burner radius is used to normalize lengths.

tially premixed front; determined by the rate of strain and gradient of mixture fraction imposed upon it, and the amount of heat released by combustion. Increasing the curvature reduces the flame speed. The effect

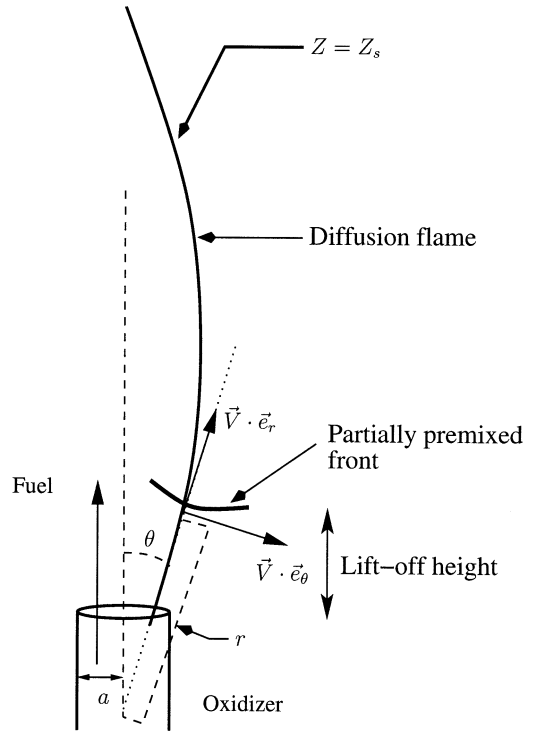


Fig. 2. Coordinates used in Landau [29] solution for laminar round jet issuing into a stagnant atmosphere.

of the heat release is the deflection of the flow upstream of the curved front, which has the net result of making the triple-flame propagate faster than S_L^o , the propagation speed of a fully premixed and planar stoichiometric flame. This flow deflection also induces a decrease of the mixture fraction gradient in the trailing diffusion flame [16]. The velocity of the overall triple flame structure is therefore greater than the premixed burning velocity, however, in a frame in which the triple flame is stationary, the flow slows down near the triple flame tip, to a velocity close to S_L^o . Knowledge is thus available on the effect of heat release in the planar triple-flame configuration, the main objective of this paper is to investigate the effect of heat release when the triple-flame propagates in an axisymmetric flow.

Flames lifted in laminar axis-symmetric (round) jets have been studied using a variety of techniques [18–23]. The principal observation is that, when the mass flow rate exceeds a critical value, the base of the diffusion flame lifts off from the burner exit. The flame base is expected to be in the vicinity of the point where the flow velocity, measured along the stoichiometric surface, is approximately the triple-flame velocity. Based on this idea, and neglecting for the moment any flow perturbations caused by the

Table 1

Criteria used to define the flame base location. S_L° is the premixed flame burning velocity, $\mathcal{F}(\chi_s)$ and $\mathcal{F}_\alpha(\chi_s)$ are corrections for curvature of the partially premixed flame front and α is the heat release parameter (see Eq. 5, 6 and 7)

Case	Criteria	Flame base velocity
I	Stoichiometric planar premixed flame	$U_{F_b}^I = S_L^\circ$
II	Triple flame with curvature	$U_{F_b}^{II} = S_L^\circ - \mathcal{F}(\chi_s)$
III	Triple flame with curvature and heat release	$U_{F_b}^{III} = S_L^\circ(1 + \alpha) - \mathcal{F}_\alpha(\chi_s)$

heat release effect, the flame base is expected to be at the intersection of the stoichiometric line with a line indicating a flow velocity of S_L° , the stoichiometric burning velocity. The Schmidt number of the fuel, S_c , determines the relative position between iso-velocity and iso-mixture fraction surfaces; the evolution of the flow velocity along the stoichiometric surface therefore depends on S_c . The response of the flame base to variations in jet Reynolds number is consequently strongly related to S_c and has motivated further studies [23–25] in that direction.

Notwithstanding its importance, a careful study of the impact of heat release on the physical analysis of lifted flames in laminar round jets has not been undertaken. As in the two-dimensional mixing layer, heat release induces flow deflection slightly upstream of the triple-flame. This may result in modifications of the topology of the iso-velocity and iso-mixture fraction surfaces so that the location of the edge of the lifted flame is altered. This aspect of laminar lifted flames is investigated here using numerical simulations of the primitive balance equations. Figure 1 displays an overview of the simulations for a given level of heat release.

Two sets of lifted flames are obtained by varying the level of heat release in the computations. For the same jet Reynolds number, it is found that the lift-off height changes significantly when the level of heat release is varied. In the light of these numerical results, the physical mechanisms controlling the subtle coupling between heat release and the axisymmetric triple-flame position are examined. It is observed that the flame stabilizes itself along the stoichiometric line, where the local flow velocity is close to S_L° , the stoichiometric premixed flame velocity. However, the exact location of the line of intersection of these two iso-surfaces is governed by the level of heat release. The effect of heat release increases with the lift-off height, as a direct consequence of the strong evolution of the shape of the triple-flame when the suspended flame moves downstream [21]. For each jet Reynolds number, one may estimate the length between the burner exit and the point where the iso-stoichiometric surface meets the axis of symmetry. Blowout is expected at a Reynolds number

where the lift-off height is close to this length, which is modified by heat release also. Therefore, the critical blowout condition is found to be affected by density change.

Arguing that the characteristic thickness of the preheat zone in front of the flame is more than an order of magnitude smaller than the lift-off height, cold flow jet theories have been used in the past to determine both the flow field upstream of the flame base and the flame base location [21,24,25]. A direct comparison is made between the flame position provided by the simulations and cold flow jet theories. The results confirm that the flame base position depends on the amount of heat release and that the magnitude of the effect varies with the jet Reynolds number.

In the subsequent sections, the flow configuration and the numerical procedure are first presented. The behavior of the lift-off height and its response to heat release are then investigated. Comparisons are also conducted between the predictions obtained by the cold flow theory, for three levels of approximation, the numerical simulations and the experiment by Chung and Lee [24]. From the results, the various effects of heat release on lifted flames are further investigated.

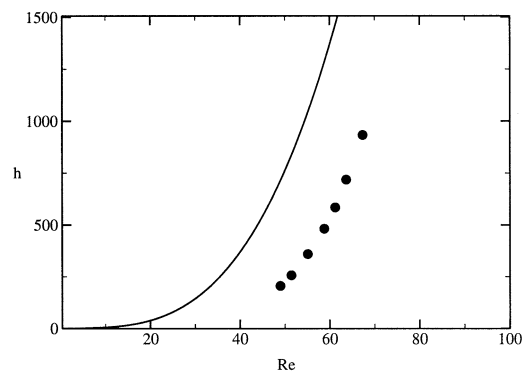


Fig. 3. Comparison between cold flow theory $h = h^{III}$ (line) and measurements by Chung and Lee [24] (full circles). Lengths are normalized by the jet radius.

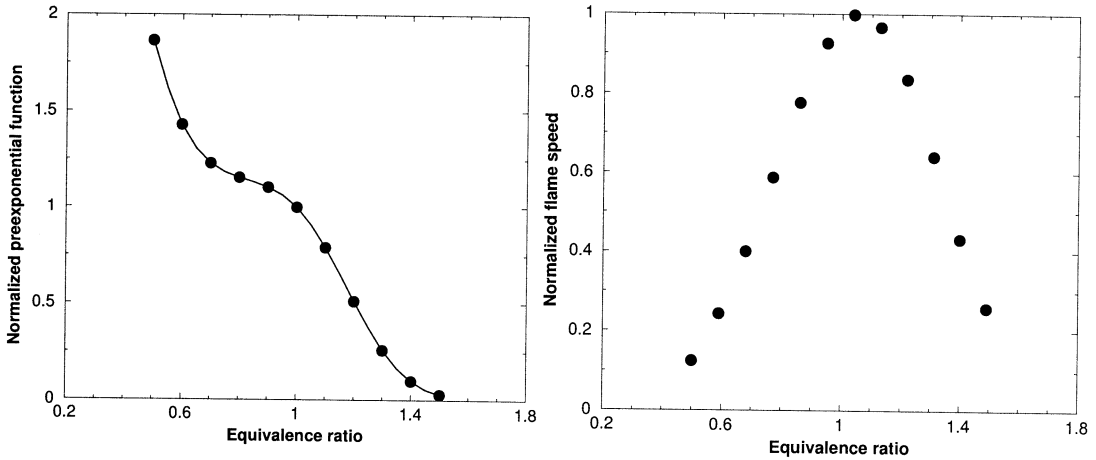


Fig. 4. Left: Preexponential function $A(\phi(Z))$. Right: Flame speed $S_L(\phi(Z)) / S_L^0$, versus equivalence ratio of the mixture $\phi(Z) = \phi_o Z / (1 - Z)$.

2. Analytical approximations for the lift-off height

Approximations of lift-off heights are discussed in this section, they are based on a description of the flow velocity that does not account for heat release. To our knowledge, a flow solution upstream of a flame base accounting for heat release is not yet available. From this point, simulations are performed using a numerical procedure organized so that any deviation from the standard cold-flow solution can be fully attributed to heat release effects.

Analytical solutions for a variety of jet flow problems have been developed under various approximations [26]. These could provide useful approximations to the velocity and mixture fraction fields in laminar jets, though not all of the assumptions behind these analytical solutions are necessarily realized in the region where the flame based is localized. Specifically, the flame base may be located too close to the jet orifice so that the laminar boundary layers are not fully developed and the “far field” approximation is not fully realized. Such solutions may nevertheless still be useful for the purpose of developing approximate expressions for lift-off heights [18,21,24] that exhibit the right scaling though they may not be accurate in detail.

We use as our starting point, the problem of the laminar jet from a point source of momentum, which was solved in the context of the boundary layer approximation for slender jets by Schlichting [27] and later solved exactly by Landau [28,29] and also by Squires using a similarity transformation [30]. This solution is best written with respect to a spherical polar co-ordinate system shown in Fig. 2. We denote the radius of the burner nozzle by a and let F_*

be the flux of jet momentum. The corresponding jet Reynolds number is:

$$Re = \left(\frac{F_*}{2\pi\rho\nu^2} \right)^{1/2} \tag{1}$$

where ρ is the density and ν the kinematic viscosity of the mixture. The parameter $\theta_o = (32/3)^{1/2} Re^{-1}$ is often used in place of the Re , it indicates the opening angle of the jet. Then, in the limit of large Re , the radial velocity in the spherical coordinates may be expressed as [29]:

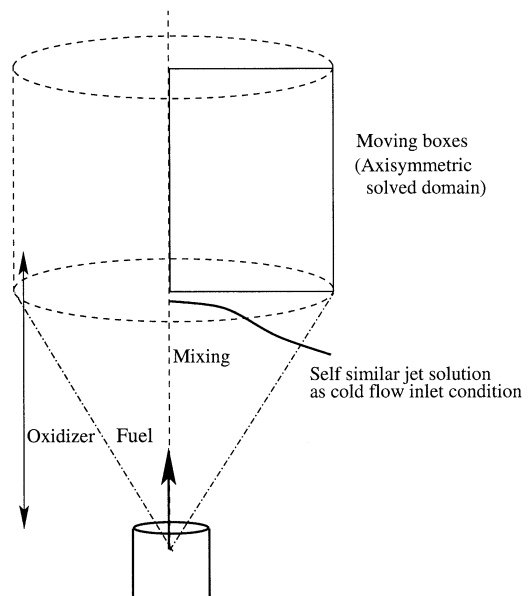


Fig. 5. Schematic of the computational domain.

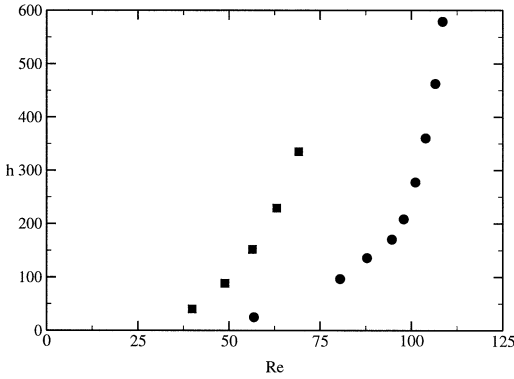


Fig. 6. Lift-off heights of the laminar flame base for two different heat release factors. Circle: $\tau = 5$ ($\alpha = 0.8$). Square: $\tau = 1.4$ ($\alpha = 0.3$). Heights are normalized by the jet radius.

$$\vec{V} \cdot \vec{e}_r = \frac{8\nu\theta_0^2}{(\theta_0^2 + \theta^2)^2 r} \quad (2)$$

The mixture fraction field may be written as [29]:

$$Z = \frac{a}{\theta_0 T} \left(\frac{\theta_0^2}{\theta_0^2 + \theta^2} \right)^{2S_c} \quad (3)$$

The Schmidt number of the fuel is set to $S_c = 1.3$ in this study, for both analytical approximation and simulations. (Schmidt number of propane is usually considered of the order of 1.376 [18]). The Lewis number is set to unity.

Other components of the velocity field are assumed small compared to $\vec{V} \cdot \vec{e}_r$. Accordingly, the azimuthal contribution of the mixture fraction gradient is supposed to control the mixture fraction dissipation rate:

$$\chi_s \approx \left(\frac{\lambda}{\rho C_p} \right) \left(\frac{1}{r} \frac{\partial Z}{\partial \theta} \right)_s \quad (4)$$

where λ and C_p are the thermal conductivity and specific heat at constant pressure of the gas and unit Lewis numbers have been assumed. The subscript s denotes stoichiometric conditions.

We will regard the laminar flame base to form an edge-flame (or triple-flame) and propagate in the vicinity of the stoichiometric surface at a given speed U_{F_b} , the edge-flame velocity in stationary fluid. Three levels of approximation for the lift-off heights may be made by choosing three different expressions for U_{F_b} , that are denoted by $U_{F_b}^I$, $U_{F_b}^II$ and $U_{F_b}^III$ (Table 1). The first and the second approximations do not account for heat release, while the third is an attempt to include some of the flow modifications due to gas expansion. The second and the third expressions for the flame velocity account for the curvature of the

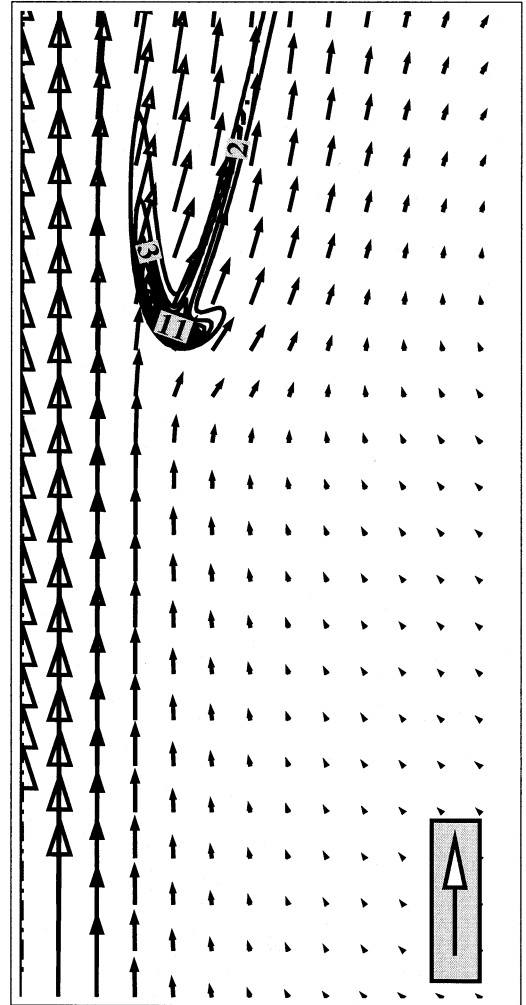


Fig. 7. Snapshot of the flow deflection upstream of the axis-symmetric flame base for $\tau = 5$ and $Re = 57$. Horizontal: radial coordinate τ . Vertical: Streamwise coordinate. Size of the visualized domain in characteristic planar unstrained stoichiometric and laminar premixed flame thickness 20×33 . Iso-heat release rate normalized by the maximum burning rate of a laminar premixed flame, iso-2: 0.12, iso-3: 0.24, iso-11: 0.92. Velocity vectors: the vertical arrow scales $10S_L^o$.

partially premixed front that constitutes the flame base.

The lowest level approximation assumes that the flame base propagates at a velocity S_L^o , the stoichiometric planar flame speed:

$$U_{F_b}^I = S_L^o \quad (5)$$

This approximation does not account for the curvature of the flame edge or density variations due to heat release. The effect of curvature of the partially

premixed front is incorporated in $U_{F_b}^{II}$ and $U_{F_b}^{III}$, where U_{F_b} is the triple-flame speed as a function of χ_s , the mixture fraction dissipation rate just ahead of the flame. Various approximations for the triple-flame speed as a function of χ_s are available in the literature. The first was proposed by Dold [9] and Hartley and Dold [10] based on an asymptotic theory valid for large Zeldovich numbers. Other analyses of edge-flame propagation speeds may be found in the literature [13,31,32]. Because of the mathematical complexity of this problem, no solution based on a fully satisfactory rigorous analysis has been found.

The second, $U_{F_b}^{II}$, and third, $U_{F_b}^{III}$, levels of approximation are based on an approximate solution to the triple flame problem due to Ghosal and Vervisch [14]. Their solution is derived by first approximating the curved premixed front by a parabola of unknown curvature. An exact solution to the outer problem can then be written down as a series expansion in parabolic cylinder co-ordinates. Matching with the reaction zone then determines the propagation speed and curvature. The above closed form solution that assumes constant density can then be “perturbed” by assuming a small heat release to derive a “corrected” outer solution. The matching conditions at the reaction zone then determines the lowest order corrections to the curvature and propagation speed when the heat release is small. Their approximation $U_{F_b}^{II}$ accounts for the curvature of the partially premixed front due to variations of the mixture fraction gradient but neglects gas expansion [14]:

$$U_{F_b}^{II} = S_L^o - \mathcal{F}(\chi_s) \quad (6)$$

where $\mathcal{F}(\chi_s) = \mathcal{A}\chi_s^{1/2}$ is a correction for the curvature of the partially premixed front, with $\mathcal{A} = \beta/(Z_s\sqrt{4\nu_F - 2}) (\lambda/\rho C_p)^{1/2}$. Where β is the Zeldovich number, ν_F is the molar stoichiometric coefficient of the fuel (assumed to be equal to that of the oxidizer) and Z_s is the value of the mixture fraction variable at stoichiometric conditions (notations are as in [33]). Correcting for heat release results in the third expression $U_{F_b}^{III}$ which may be written [14] as:

$$U_{F_b}^{III} = S_L^o(1 + \alpha) - \mathcal{F}_\alpha(\chi_s) \quad (7)$$

where $\mathcal{F}_\alpha = \mathcal{A}_\alpha\chi_s^{1/2}$ with $\mathcal{A}_\alpha = \mathcal{A}/(1 + \alpha)$. The heat release factor $\alpha = (T_s - T_o)/T_s$ is defined from T_s , the temperature of the stoichiometric fully burnt products measured when fuel and oxidizer are both initially at the reference temperature T_o .

The flame base location and the lift-off height are then obtained by looking for the condition $U_{F_b}^i = \tilde{V} \cdot \tilde{z}_r$ on the stoichiometric surface (when $i = I, II$ or III). Imposing this requirement by using Eq. (2) and (3) leads to an equation for the variable $x = (\theta/\theta_o)$ [25], where θ is the angular position of the flame base:

$$(1 + x^2)^{2S_c - 2} [1 + A^i x(1 + x^2)] = B^i \quad (8)$$

For the three levels of approximation discussed earlier, (Eq. 5, 6 and 7):

$$\begin{aligned} A^I &= 0 & B^I &= \frac{\theta_o a}{8Z_s S_c (\lambda/\rho C_p)} S_L^o \\ A^{II} &= \frac{\beta \theta_o}{2\sqrt{4\nu_F - 2}} & B^{II} &= B^I \\ A^{III} &= \frac{A^{II}}{(1 + \alpha)} & B^{III} &= B^I(1 + \alpha) \end{aligned}$$

Eq. (8) is therefore a transcendental equation for $i = II$ and III , whose solutions are denoted x^i . The lift-off height is directly related to x^i as may be inferred from Fig. 2 using elementary geometry:

$$h^i = r(x^i \theta_o)_s \cos(x^i \theta_o) - \frac{a}{\theta_o} \quad (9)$$

Here $r(x^i \theta_o)_s$ is the radial coordinate of the flame base and a/θ_o is the correction accounting for the virtual origin. For given chemical parameters, S_L^o , β , α and Z_s , Eq. (8) and (9) may be used to predict a lift-off height h^i , for various values of Re .

Careful measurements of lift-off heights were performed by Chung and Lee [24] for various fuels. They reported that analytical expressions for h follow an empirical law of the form:

$$h = A(Re)^B \quad (10)$$

where A and B are two empirical constants determined to match experimental results, B being modified when the Schmidt number of the fuel varies. The cold-flow mixing theory can indeed be fitted using such law and similar types of approximations were proposed by Chen and Bilger [21]. To improve these approximations, the careful prediction of the flow was recently addressed by Revuelta et al [22, 34], but still for uniform temperature. So far, these approximations are known to lack of prediction capabilities, when not only trends but absolute values of lift-off heights need to be predicted. This is illustrated in Fig. 3 where a comparison is performed between measurements by Chung and Lee [24] and prediction of h as obtained using $U_{F_b}^{III}$.

3. Numerical simulations of the flame zone

Numerical simulations of the compressible flow equations coupled with the equations for temperature and species are performed in a limited region around the triple flame. Upstream of this computational region, the flow is assumed to be the cold flow solution

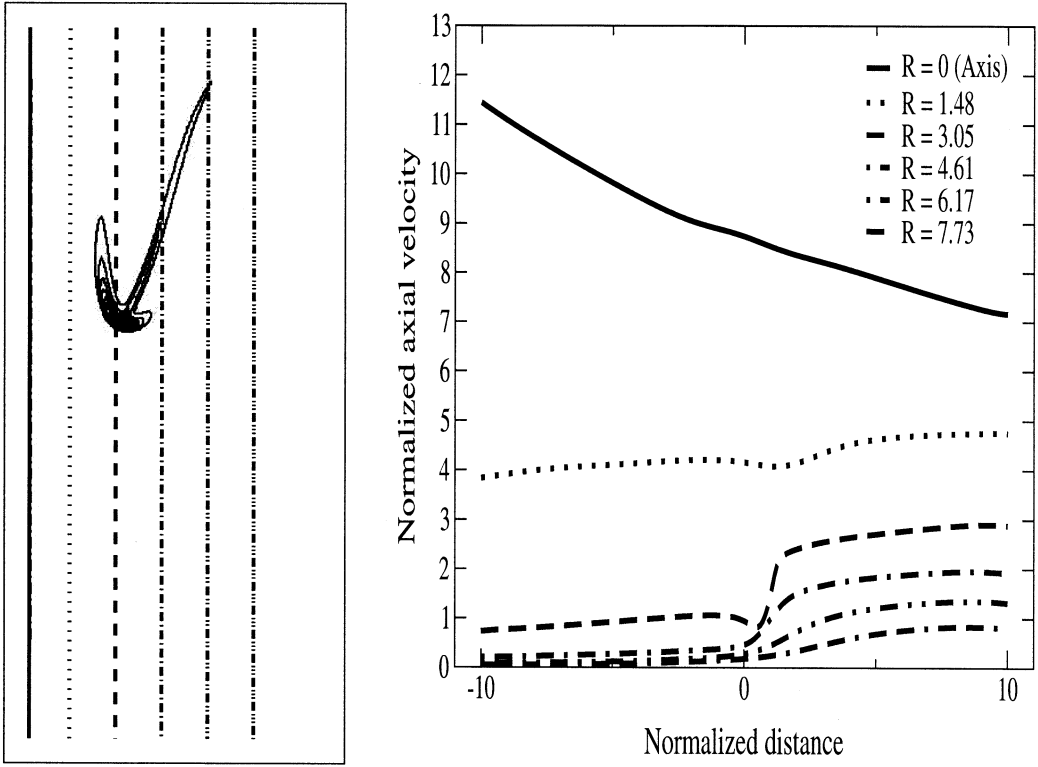


Fig. 8. Left: Iso-heat release rate, case $Re = 57$ and $\tau = 5$. Right: Velocity profiles along the streamwise direction for the various radial positions displayed on left. Velocity is normalized by S_L^o . R: Normalized radial position.

for the Landau-Squire jet discussed above. This procedure saves a great deal of computational time and allows for comparing the cold-flow theory of lifted flames with simulations under the same framework. But on the other hand, the predictive capabilities of the simulations are restricted. Only the correction to the lift-off height, h , due to the impact of heat release effects can be computed. In addition, the computations would not be reliable in describing flames lifted very close to the burner, because, the self-similar solution is not valid in the close field of the round jet. The full simulation would require a careful description of both the laminar round jet boundary layers and the far field, a task that is difficult to achieve together with the accurate fully compressible Direct Numerical Simulation (DNS) of the flame base.

Numerical simulations of laminar lifted flames are performed using a DNS tool previously developed for studying turbulent combustion [35–38]. The DNS procedure follows well established methods [39]. The fully compressible Navier Stokes equations are solved using a sixth order PADE scheme [40] combined with third order Runge-Kutta time stepping and Navier Stokes characteristic boundary conditions (NSCBC) [41]. The possibility of dealing with axi-

symmetric configurations was introduced in the DNS solver to compute round jet diffusion flames.

All simulations are parametrized with the jet Reynolds number, Re , defined by (Eq. 1). Lift-off heights and all lengths are normalized by a , the jet radius; velocities are normalized by S_L^o , the stoichiometric planar premixed flame burning velocity. The chemical source term is taken as a single-step Arrhenius law. In the numerical simulations, the activation temperature, T_{A_c} is fixed, and its value may be inferred from the Zeldovitch number $\beta = (T_{A_c}/T_s)\alpha = 8$. The equivalence ratio is $\phi_o = 15$, ϕ_o corresponds to the equivalence ratio obtained when premixing the same mass of fuel and oxidizer streams, leading to a stoichiometric point $Z_s = 1/(1 + \phi_o) = 0.0625$. Single-step kinetics lack of reaction pathway involving radical species and are known to overestimate the flame speed and the burning rate for rich conditions [33]. To overcome this strong limitation, which could easily generate an artificial fuel-rich wing, the pre-exponential constant is a function of the mixture fraction. This function is determined so that the flame speed reproduces a typical hydrocarbon behavior. The burning rate is thus expressed as:

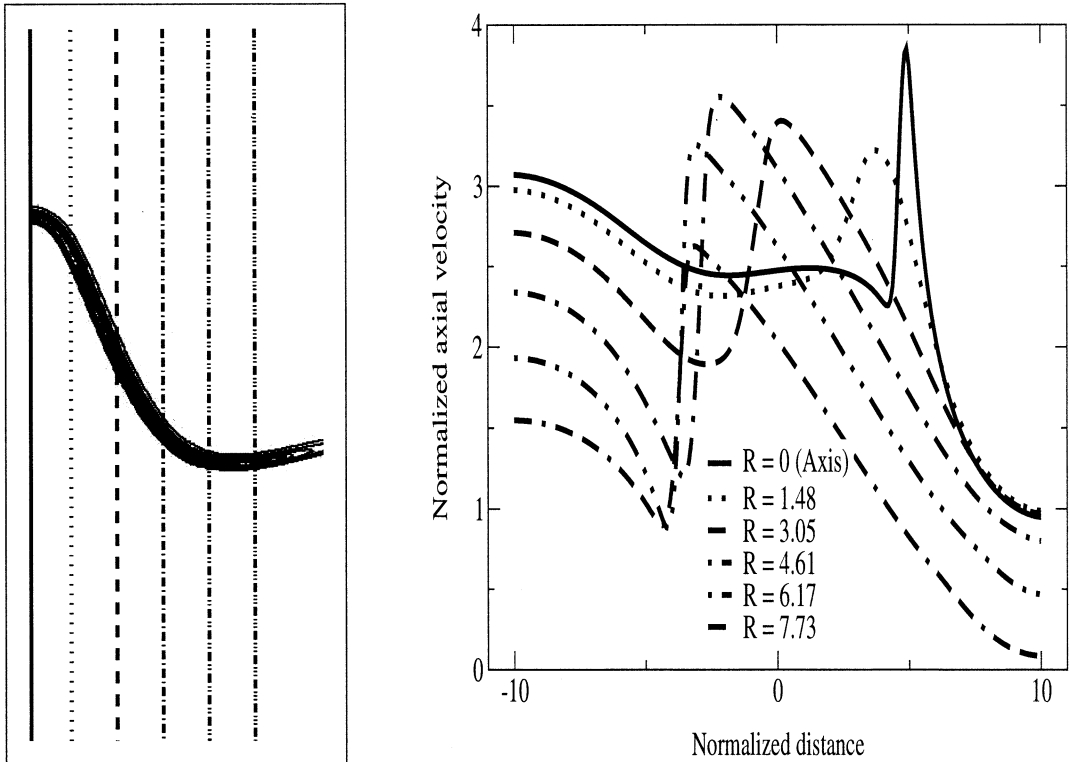


Fig. 9. Left: Iso-heat release rate, case $Re = 104$ and $\tau = 5$. Right: Velocity profiles along the streamwise direction for the various radial positions displayed on left. Velocity is normalized by S_L^c . R: Normalized radial position.

$$\dot{\omega} = K_o A(Z) Y_F Y_O^2 \exp(-T_A/T) \quad (11)$$

The function $A(Z)$ is optimized from simulations of premixed laminar and planar flames using a procedure reported elsewhere [42]. K_o calibrates the maximum value of the flame speed, while $A(Z)$ ensures the proper response versus equivalence ratio. Figure 4 shows the flame speed response and the corresponding $A(Z)$. A typical hydrocarbon flame speed response is recovered [43].

The simulations are performed within the domain depicted in Fig. 5. When the jet Reynolds number, and therefore the lift-off height, changes, the domain is shifted so as to contain the flame base within the domain boundaries. As shown in Fig. 5, the domain is axisymmetrical in shape, of physical size $10a$ in the radial direction and $20a$ in the vertical direction. The grid consists of a 257×128 uniform mesh. The various downstream locations of the domain are estimated prior to the simulations through approximated lift-off heights, in order to position the computational domain appropriately, a first estimate of the flame base position is obtained using the cold-flow analysis, for each simulation it is based on the lift-off height provided by the criterion $U_{F_b} = S_L^c$

(Table 1). Because frozen flow mixing upstream of the flame base is not computed, the self-similar Landau-Squire solution is used to provide inlet conditions for velocities and mixture fraction. Great care is taken to ensure that the inlet of the computational domain is far enough from the flame base, to avoid any spurious coupling between the cold flow inlet conditions and the burning zone.

The consistency of this procedure of obtaining the inlet conditions from the Landau-Squire solution for the DNS solver is first tested by performing a simulation without combustion for a jet with $Re = 40$. When the cold flow theory is used as inlet, there is almost no difference between the DNS solution in the computational domain and the self-similar analytical solution. Of course, this test does not necessarily tell us that the Landau-Squire solution correctly describes the flow and mixture fraction fields in the region of interest. It merely indicates that the Landau-Squire solution is a good approximation to the solution of the boundary value problem for our limited computational domain. The former conclusion may only be drawn based on a full numerical solution of the jet, a task that we carefully avoid by restricting

our simulation to a limited region around the flame base. However, this test does assure us, that in the presence of a flame, any deviation of the flow and mixture fraction concentration from the Landau-Squire solution can be fully attributed to gas expansion effects resulting from the heat released in the combustion. Flames stabilized at a downstream location further than 10 jet radius from the source are considered, since, the self-similar jet solution is not reliable for locations closer than this to the jet orifice.

4. Heat release effects on laminar lifted flames

The lift-off height obtained from the DNS is plotted against the jet Reynolds number, Re , in Fig. 6. The lift-off height is measured using the maximum reaction rate on the stoichiometric surface, at the location of the burning rate of the premixed kernel. It has been verified that the burning rate always decays, from this point, in the trailing diffusion flame.

Two values of the heat release parameter α are considered, $\alpha = 0.3$ and $\alpha = 0.8$. They correspond to a ratio of temperatures across a stoichiometric premixed flame $\tau = (T_s/T_o) = (1 - \alpha)^{-1}$ that is equal to 1.4 and 5, respectively. The pre-exponential constant K_o , of the single-step Arrhenius chemistry, differs in the two sets of calculations, so that the reference stoichiometric and planar premixed flame velocity, S_L^o , is kept constant when varying τ . The change of the fuel in an experiment would modify more parameters than only the amount of heat release. The flame speed and the Schmidt number would also be modified, leading to the very intricate laminar lifted flame problem. The choice of generating synthetic flames, where α is modified only, is made to isolate the impact of heat release. This restricts the scope of the study, but the differences between the two sets of calculations can be then attributed fully to the different amount of heat released by fuel oxidation.

Before the blow-out condition, all the flame base locations are closer to the burner for $\tau = 5$ than for $\tau = 1.4$ (Fig. 6). For each distribution of lift-off heights, the point obtained for the highest Re corresponds to near blow-out conditions. For $\tau = 1.4$, blow-out occurs at $Re \approx 70$, while the flame is more robust for $\tau = 5$, with a blow-out condition observed at $Re \approx 110$. The flame can thus be suspended above the burner for higher fuel jet velocities when the amount of heat release becomes greater. The difference between the two lift-off heights $\Delta h = h_{\tau=1.4} - h_{\tau=5}$ increases with the jet velocity (Fig. 6) and this is related to a change of the flame topology when Re increases.

Figure 1, which was obtained with $\tau = 5$, shows that the structure of the flame base is strongly mod-

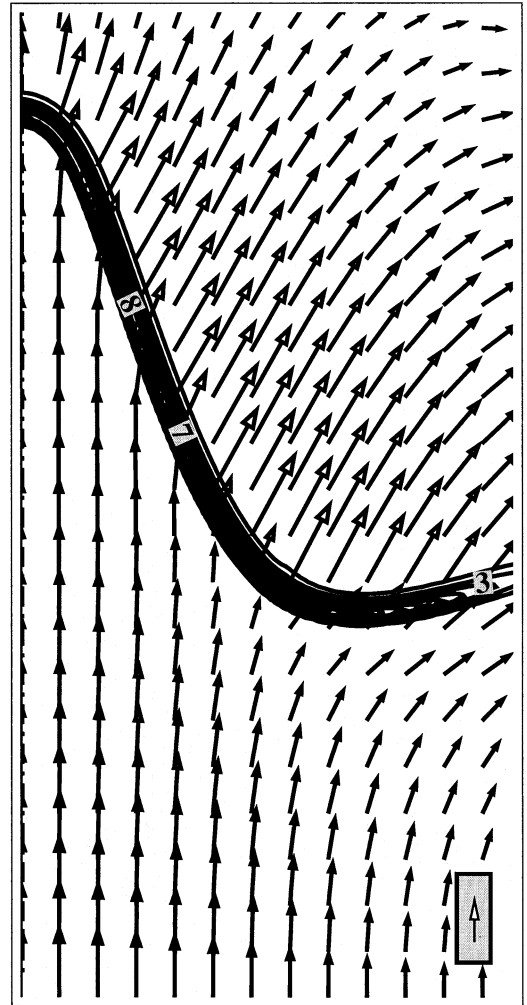


Fig. 10. Iso-burning rate and velocity vector field. $Re = 104$ and $\tau = 5$. Horizontal: radial coordinate τ . Vertical: Streamwise coordinate. Size of the visualized domain in characteristic planar unstrained stoichiometric and laminar premixed flame thickness 20×33 . Iso-heat release rate normalized by the maximum burning rate of a laminar premixed flame, iso-3: 0.18, iso-7: 0.42, iso-8: 0.5. Velocity vectors: the vertical arrow scales $3S_L^o$.

ified when the lift-off height increases. For moderate values of h , the flame takes the form of a triple-flame featuring a partially premixed front with a trailing diffusion flame. The partially premixed front progressively grows when the flame base moves downstream, because the frozen flow mixing zone is well developed ahead of the flame (see cases $Re = 107$ and 109 in Fig. 1). Fig. 7 illustrates the flow deflection in the axi-symmetric round jet. Conservation of mass through the curved front coupled to the density jump across the reaction zone induces a flow deflec-

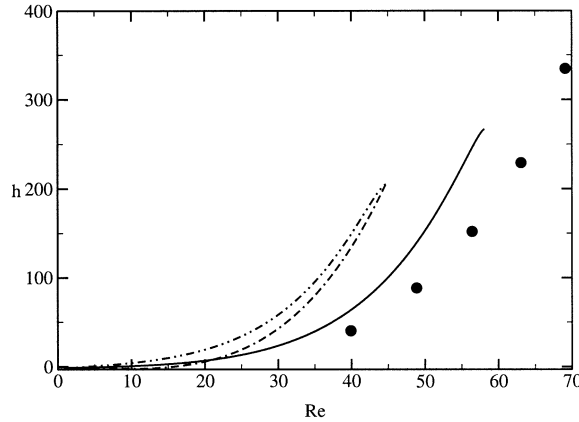


Fig. 11. Lift-off heights for $\tau = 1.4$. Circle: Numerical simulations. Dash double dot: Approximation using $U_{F_b}^I = S_L^\circ$. Dash dot: Approximation using $U_{F_b}^II = S_L^\circ - \mathcal{F}(\chi_s)$. Line: Approximation using $U_{F_b}^III = S_L^\circ(1 + \alpha) - \mathcal{F}_\alpha(\chi_s)$ (Table 1).

tion [16] ahead of the flame base, which is accompanied by a flow redirection downstream of the burning zone. This effect is enhanced for large values of the lift-off height, since the partially premixed front is much more developed. Figures 8 and 9 show the burning rate and streamwise velocity profiles through the flame base for the cases $Re = 57$ and $Re = 104$, respectively. Typical “triple-flame velocity profiles” are observed across the premixed kernel for $Re = 57$ (Fig. 8), with a minimum velocity of the order of S_L° . The flow modification due to heat release in this case is localized in the immediate vicinity of the flame base. Away from the flame, on the axis of symmetry and on the fresh air side, the velocity is almost not perturbed by the burning zone. The volume of flow affected by the flame base is much larger for $Re = 104$ (Fig. 9), where the flame is further downstream. In this case, the flame base touches the axis of symmetry and it “opens up” the top of the jet through a large induced flow deflection (Fig. 10). Nevertheless, the velocity at the location of the maximum burning rate remains very close to S_L° , the stoichiometric and planar premixed flame velocity. The corresponding upstream velocity is of the order of $2S_L^\circ$, as observed in experiments with laminar and turbulent lifted flames [1,4]. The increase of Δh with the fuel jet velocity is thus a direct result of heat release induced modification of the flow field.

To quantify more carefully heat release induced effects, the lift-off heights extracted from the simulations are compared to those obtained by solving Eq. (9) for the three expressions retained for U_{F_b} , the characteristic flame base velocity (Eq. 5, 6 and 7, Table 1). Close to blow-out, the mixture fraction gradient is weak and the impact of the correction $\mathcal{F}(\chi_s)$ on the flame propagation velocity becomes

negligible. Expressions of the flame base velocity that do not account for heat release, $U_{F_b}^I$ and $U_{F_b}^II$, therefore predict blow-out for the same Reynolds number as seen in Figs 11 and 12. Even though the flame is stabilized at the location where $U_{F_b} \approx S_L^\circ$ (Fig. 8 and 9), the simulations predict lift-off heights smaller than those of the analytical approximations that neglect heat release. It is also observed that the heat release helps the flame sustain much larger jet velocities than expected, with blow-out occurring for higher Re than predicted by cold flow theory. The comparison between Fig. 11 and 12 indicates that the discrepancy between the analytical predictions of lift-off heights and those calculated by DNS increases with the amount of heat release, for the two levels of approximations that neglect heat release (I and II of

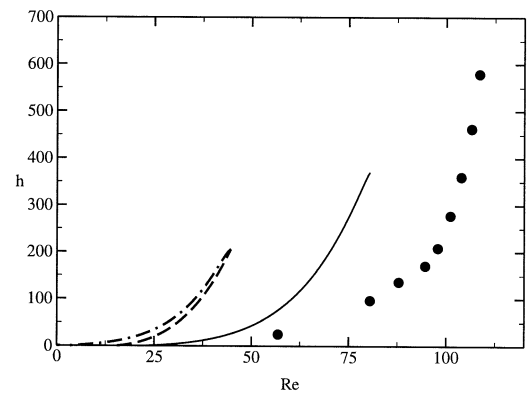


Fig. 12. Lift-off heights for $\tau = 5$. Circle: Numerical simulations. Dash: Approximation using $U_{F_b}^I = S_L^\circ$. Dash dot: Approximation using $U_{F_b}^II = S_L^\circ - \mathcal{F}(\chi_s)$. Line: Approximation using $U_{F_b}^III = S_L^\circ(1 + \alpha) - \mathcal{F}_\alpha(\chi_s)$ (Table 1).

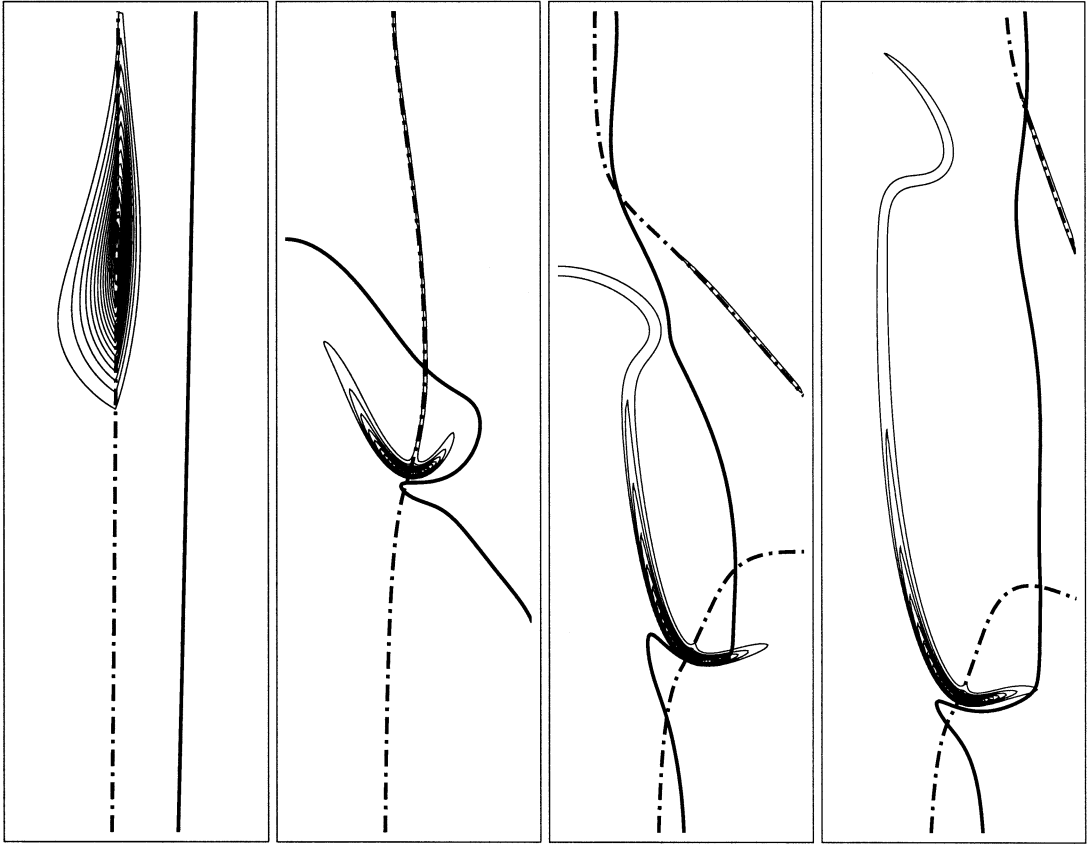


Fig. 13. Ignition of the simulation followed by an upstream edge flame movement. Iso-heat release rate. Line: $U = S_L^o$. Dotted: $Z = Z_s$. Horizontal: radial coordinate r . Vertical: Streamwise coordinate.

Table 1). The introduction of heat release effects into the flame base velocity ($U_{F_b}^{III}$, Eq. 7) modifies the prediction of lift-off heights. The analytically predicted flame base location comes closer to the simulations for $\tau = 1.4$. Since the theoretical development was conducted for small values of α ($\tau \approx 1$) [14] it cannot be expected to capture fully the large heat release effects found in Fig. 12 that was obtained with $\tau = 5$.

Theoretical predictions of lift-off heights, including the three levels of approximations discussed above, are based on the premise that the flame tip locates itself on the stoichiometric surface at a point where the flow velocity is close to the value S_L^o . The flow velocity measured in the simulations at the flame base is indeed very close to S_L^o . However, the lift-off height calculated on this assumption does not match the DNS results very well. This is only possible, if the flow perturbation due to the edge flame significantly alters the velocity and species distribution of the cold flow theory changing the location of the stoichiometric surface and/or the position where

the flow velocity equals S_L^o . Since the simulated flames are observed upstream from their expected theoretical positions (Fig. 11 and 12), we must conclude that the edge-flame must modify the mixture locally in order to establish this stabilization point.

Figure 13 attempts to capture the dynamic process of the relative movement of iso- S_L^o and iso- Z_s surfaces, by which the new equilibrium position gets established. A sequence of images following ignition is shown for a representative simulation. On the stoichiometric line, the flame is ignited intentionally away from the expected equilibrium position where the iso- S_L^o and iso- Z_s meet in the round jet. The location of ignition is chosen in a zone where the flow velocity, on the stoichiometric surface, is larger than S_L^o . Soon after ignition, a flame base propagates at the stoichiometric burning velocity S_L^o . Both iso- S_L^o and iso- Z_s are displaced by the flame so that they come into contact at the triple point (Fig. 13). Then, an upstream flame movement is organized, where the flow deflection due to heat release continuously insures that the iso- S_L^o and iso- Z_s stay in contact at the

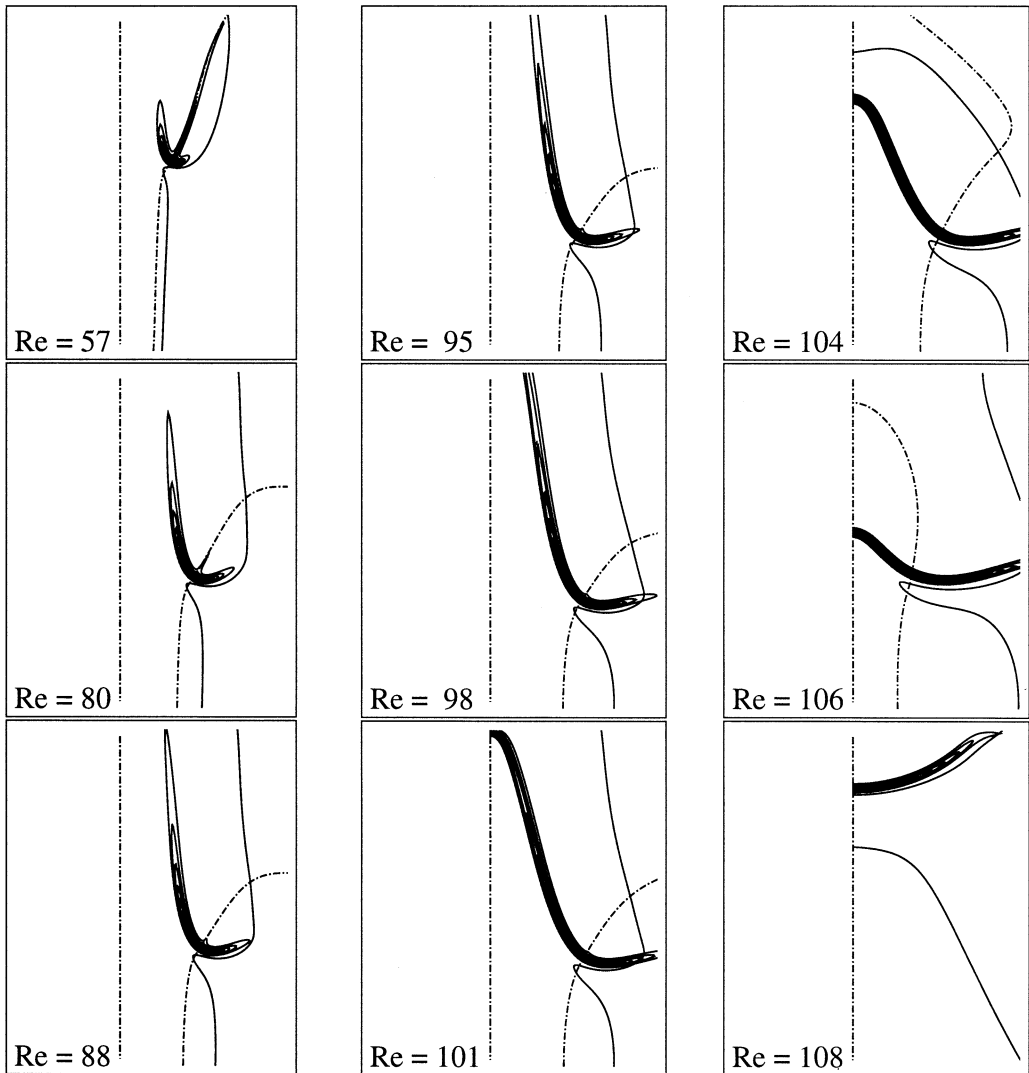


Fig. 14. Lifted flame structure for different jet Reynolds numbers, simulations with $\tau = 5$. Iso-heat release rate. Vertical dotted line: Axis of symmetry. Dotted line: $Z = Z_c$. Line: $U = S_L^0$. Horizontal: radial coordinate r . Vertical: Streamwise coordinate.

flame tip. The flame base finally stops moving upstream, when the local conditions do not allow for further propagation into the larger jet velocities. The final and steady conditions are displayed in Fig. 14 for various jet Reynolds numbers for large heat release ($\tau = 5$). The iso- S_L^0 is strongly deflected by the burning zone, so that the flame can be stabilized closer to the burner than it would be without gas expansion. The higher the fuel jet velocity, the larger the deflection between the iso-surfaces. As explained above, this is related to the modification of the flame topology when it moves downstream with increase of the jet Re . This modification of the mixture and velocity fields also helps the flame to endure much

larger jet velocity and to postpone blowout. Before blow-out, a flame burning in a lean mixture is observed (Fig. 15 for $Re = 108$). A complex flow structure is found, the iso- Z_c first touches the axis of symmetry (the iso- Z_c cannot be displayed on this particular lean combustion regime). Downstream of this point, the iso- S_L^0 meets the axis and further downstream, a lean flame covers the jet.

5. Conclusion

Numerical simulations of laminar round jet diffusion lifted flames were performed with a high order

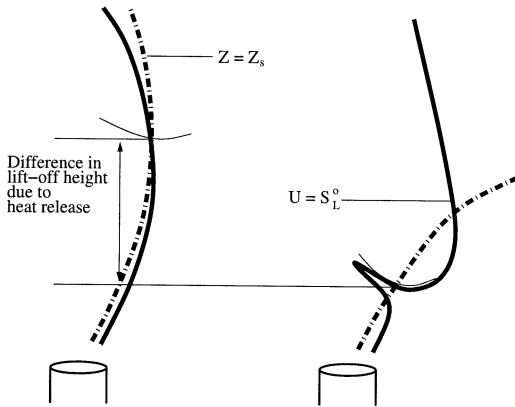


Fig. 15. Schematic of the heat release effect on lift-off height. Left: without heat release. Right: Including heat release. Line: Locations where $U = S_L^0$. Dotted: Iso-stoichiometric surface.

accurate Direct Numerical Simulation tool. Lift-off heights were compared with those obtained by combining a self-similar cold flow jet solution, with three levels of approximation for the propagating velocity of the lifted flame base. A strong discrepancy exists between predicted and simulated lift-off heights, specifically when heat release effects are not included in the theoretically estimated speed of the flame base.

The flame is always stabilized in the simulations on the stoichiometric surface, at a point where the fluid velocity is close to the stoichiometric premixed flame burning velocity. However, the exact position of the stabilization point is driven by heat release. The flow deflection resulting from heat release promotes an upstream movement in the cold flow of the point where the conditions of stabilization are encountered. This result is sketched in Fig. 15.

The flow deflection is more pronounced when the jet Reynolds number is increased. According to the numerical results, this derives from a strong modification of the structure of the simulated flame base depending on its downstream position. When the flame base moves downstream with the increase of fuel jet velocity, edge-flames or triple-flames with a burning trailing diffusion flame develop gradually into a large partially premixed front that deeply modifies the cold flow frozen flow mixing upstream of the burning zone. The blowout conditions are thus observed for much larger fuel jet velocity that predicted by any cold flow theory. Some of these effects may certainly persist in turbulent lifted flame bases.

These observations suggest that it would be necessary to include effects of heat release in the axisymmetric flow description, upstream of the flame, to improve theoretical predictions of lift-off height.

References

- [1] L. Muñiz, M.G. Mungal, *Combust. Flame* 111 (1/2) (1997) 16–31.
- [2] R.W. Schefer, P. Goix, *Combust. Flame* 112 (4) (1998) 559–574.
- [3] K.A. Watson, K.M. Lyons, J.M. Donbar, C.D. Carter, *Combust. Flame* 119 (1/2) (1999) 199–202.
- [4] C. Maurey, A. Cessou, D. Stepowski, *Proc. Combust. Inst.* 28 (2000) 545–551.
- [5] H. Phillips, Tenth Symposium (International) on Combustion, The Combustion Institute, Pittsburgh, 1965, p. 1277–1283.
- [6] P.N. Kioni, B. Rogg, K.N.C. Bray, A. Liñán, *Combust. Flame* 95 (1993) 276–290.
- [7] R. Azzoni, S. Ratti, I.K. Puri, S.K. Aggarwal, *Combust. Flame* 119 (1/2) (1999) 23–40.
- [8] S.K. Aggarwal, I.K. Puri, *Phys. Fluids* 13 (1) (2001) 265–275.
- [9] J.W. Dold, *Combust. Flame* 76 (1989) 71–88.
- [10] L.J. Hartley, J.W. Dold, *Combust. Sci. Tech.* 80 (1991) 23–46.
- [11] J. Buckmaster, M. Matalon, Twenty-second Symposium (International) on Combustion, The Combustion Institute, Pittsburgh, 1988, pp. 1527–1535.
- [12] J. Daou, A. Liñán, Twenty-Seventh Symposium (International) on Combustion, The Combustion Institute, Pittsburgh 1998, p. 667–679.
- [13] J. Daou, A. Liñán, *Combust. Theory Modelling* 2 (4) (1998) 449–477.
- [14] S. Ghosal, L. Vervisch, *J. Fluid Mech.* 415 (2000) 227–260.
- [15] J. Boulanger, L. Vervisch, *Combust. Flame* 130 (1) (2002) 1–14.
- [16] G. Ruetsch, L. Vervisch, A. Liñán, *Phys. Fluids* 6 (7) (1995) 1447–1454.
- [17] T. Echehki, J.H. Chen, *Combust. Flame* 114 (1/2) (1998) 231–245.
- [18] B.J. Lee, S.H. Chung, *Combust. Flame* 109 (1) (1997) 163–172.
- [19] O. Savas, S.R. Gollahalli, *J. Fluid Mech.* 165 (1986) 297–318.
- [20] T. Plessing, P. Terhoeven, N. Peters, M.S. Mansour, *Combust. Flame* 115 (3) (1998) 335–353.
- [21] Y.-C. Chen, R.W. Bilger, *Combust. Flame* 123 (1/2) (2000) 23–45.
- [22] A. Revuelta, A.L. Sanchez, A. Liñán, *Combust. Flame* 128 (3) (2002) 199–210.
- [23] J. Lee, S.H. Chung, *Combust. Flame* 127 (4) (2002) 2194–2204.
- [24] S. Chung, B. Lee, *Combust. Flame* 86 (1) (1991) 62–72.
- [25] S. Ghosal, L. Vervisch, *Combust. Flame* 124 (4) (2001) 646–655.
- [26] G.K. Batchelor, *An Introduction to Fluid Dynamics*, Cambridge University Press, Cambridge, UK, 1993.
- [27] H. Schlichting, *Zeitschr. f. angew. Math. u. Mech.* 13 (1933) 260–263.
- [28] L.D. Landau, *Dokl. Akad. Sci. URSS* 43 (1944) 286–288.

- [29] L. Landau, E. Lifchitz, *Fluid Mechanics*, Pergamon Press, New York, 1987.
- [30] H. Squire, *Quart. J. Mech. Appl. Math.* 4 (3) (1951) 321–329.
- [31] J. Buckmaster, *Combust. Sci. Tech.* 115 (1996) 41–68.
- [32] J. Buckmaster, A. Hegab, TL Jackson, *Phys. Fluids* 12 (12) (2000) 1592–1600.
- [33] Poinso, T. and Veynante, D. *Theoretical and Numerical Combustion*. R. T. Edwards, Inc., 2001.
- [34] A. Revuelta, A.L. Sánchez, A. Liñán, *Phys. Fluids* 14 (6) (2002) 1821–1824.
- [35] P. Domingo, L. Vervisch, *Twenty-Sixth Symposium (International) on Combustion*, The Combustion Institute, Pittsburgh, 1996, p. 233–240.
- [36] L. Vervisch, T. Poinso, *Annu. Rev. Fluid Mech.* 30 (1998) 655–692.
- [37] J. Réveillon, L. Vervisch, *Combust. Flame* 121 (1/2) (2000) 75–90.
- [38] V. Favier, L. Vervisch, *Combust. Flame* 125 (1/2) (2001) 788–803.
- [39] T. Poinso, S. Candel, A. Trouvé, *Prog. Energy Combust. Sci.* 12 (1996) 531–576.
- [40] S.K. Lele, *J. Comput. Phys.* 103 (1992) 16–42.
- [41] T. Poinso, SK. Lele, *J. Comput. Phys.* 1 (101) (1992) 104–129.
- [42] L. Vervisch, B. Labegorre, and J. Réveillon, Submitted.
- [43] Peters, N. *Turbulent Combustion*. Cambridge University Press, 2000.